Colloids and Surfaces A: Physicochemical and Engineering Aspects 612 (2021) 126074

Contents lists available at ScienceDirect

Colloids and Surfaces A: Physicochemical and Engineering Aspects

journal homepage: www.elsevier.com/locate/colsurfa

Self-propelled sessile droplets on a superheated and heterogeneous wetting surface

Chin-Chi Hsu [a,*], You-An Lee [b,c], Chun-Hui Wu [b], C.S. Sujith Kumar [b,d]

[a] Department of Mechanical Engineering, National United University, Miaoli, 36063, Taiwan
[b] Department of Mechanical Engineering, National Taiwan University, Taipei, 10617, Taiwan
[c] Max-Planck Center Twente for Complex Fluid Dynamics, Department of Science and Technology, Mesa Institute, and J. M. Burgers Centre for Fluid Dynamics, University of Twente, P.O. Box 217, 7500 AE, Enschede, Netherlands
[d] Department of Mechanical Engineering, National Institute of Technology Calicut, Kozhikode, India

GRAPHICAL ABSTRACT

Self-propelled sessile droplet on a superheating and heterogeneous wetting surface
Fig. 2 CCD images illustrating different evaporation behaviours on the heterogeneous (mixed) wettability surface and homogeneous (hydrophobic and hydrophilic) wettability surfaces at an initial surface temperature of 140 °C. On the mixed wettability surface, droplet had the moving contact line (MCL), and droplet is moving after the static unbalance. However, the homogeneous surfaces had constant contact line (CCL) of more severe conditions of evaporation until the end of evaporation.

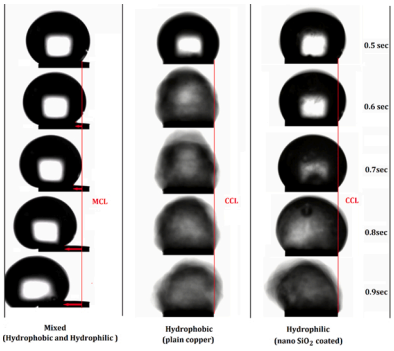

ARTICLE INFO

Keywords:
Droplet evaporation
Superheat
Hybrid
Heterogeneous
Mixed

ABSTRACT

In this study, we investigated self-propelled sessile droplet evaporation on superheated surfaces with mixed wetting patterns. The primary reason for droplet motion was an increase in surface temperature and the difference in surface energy, which affected the moving contact line and moved droplets close to the wetting regions and then out to the heating surface. In this study, we observed that increases in temperature significantly influenced the changes in surface adhesion force. The force balance equation was used to demonstrate the existence of a moment of droplet movement. In addition, temperature data demonstrated energy conservation behaviour. The heterogeneous wetting surface exhibited greater differences in energy because of the energy expended during liquid–vapour phase transition and droplet movement.

* Corresponding author.
E-mail address: cchsu@nuu.edu.tw (C.-C. Hsu).

https://doi.org/10.1016/j.colsurfa.2020.126074
Received 13 July 2020; Received in revised form 2 December 2020; Accepted 21 December 2020
Available online 28 December 2020

1. Introduction

Droplet evaporation has prominent applications in inkjet printing [1–3], biosensing [4,5], chip manufacturing [6,7], and spray cooling [8–10]. Liquid droplet evaporation on a hot solid surface can generate large amounts of heat transfer because of the latent heat, which has applications for several industrial cooling techniques. Droplet evaporation on different surfaces with homogeneous wettability, and specifically phenomena such as the cafe ring effect, Marangoni effect, and evaporating capillary meniscus, have recently attracted considerable attention. These behaviours are a result of the influence of droplet evaporation on surface wettability. Picknett and Bexon [11] first reported that droplet evaporation has three distinct stages on a general surface. During the first stage, the droplet evaporates with a constant contact radius (CCR); the radius of the droplet bead does not change, but the contact angle (CA) decreases. The first stage is called constant contact line (CCL) mode because the contact line does not move. When the CA of the droplets reaches the receding CA, the droplet enters the constant CA (CCA) phase. The CA does not change, but the radius of the liquid decreases. In the third stage, the droplet remains in a mixed coexistence condition, called the mixed mode (MM), until evaporation is complete. The evaporation situation is different for superhydrophobic or superhydrophilic surfaces. For a hydrophilic surface, the pinning effect is strong during the evaporation process. The first-stage CCR is maintained, but the droplet skips the CCA stage and directly proceeds to the MM stage. The pinning effect is weak for superhydrophobic surfaces. They enter only one MM stage in the evaporation process [12]. Studies [13,14] have revealed that surface wetting characteristics affect the evaporation rate. In their study, Dasf and Garimella [14] investigated droplet evaporation during heating of hydrophobic and superhydrophobic surfaces. Superhydrophobic surfaces exhibit slower evaporation, and the theoretical model should be corrected to apply the results of evaporation on a superhydrophobic surface.

The effects of wetting characteristics on evaporation were also observed at a micro scale. Some studies [15,16] have investigated the evaporation of microdroplets on a microcantilever and observed that the cantilever surface has hydrophilic and hydrophobic wetting properties that result in different evaporation behaviours [16]. Lee et al. [17] observed that resonance frequencies and deflections significantly differ between hydrophilic and hydrophobic anodic aluminium oxide nanoporous microcantilevers. All these studies indicated that evaporation is closely related to the homogeneous wetting characteristics of a surface. Research on evaporation on heterogeneous wetted surfaces is limited. He et al. [18] reported that the droplet evaporation rate on a heterogeneous wetting surface is greater than that on a homogeneous wetting surface. The contact line stretches on the patterns on the surface of a hydrophilic material, which enhances the diffusion area and improves the evaporation rate. The study also demonstrated that the dynamic movement of a moving contact line (MCL) increases the evaporation rate on a heterogeneous wetting surface. The depinning phenomenon on a patterned surface causes movement of the contact line. Li et al. [19] performed simulations to analyse the effects of pinning and depinning phenomena on the contact line as droplets evaporated on a heterogeneous wetting surface.

Several studies on homogeneous wetting surfaces have been conducted, characterising droplet evaporation as natural evaporation [20,21]; however, few studies have addressed droplet evaporation on heterogeneous wetting and hot surfaces. Our previous study revealed that changing the mixed (hybrid or heterogeneous) wetting characteristics of heating surfaces leads to an increase in evaporation rate during low to intermediate superheating [22]. Studies on hybrid wetting patterns have focused on the dynamic behaviour of the boiling process. However, insight obtained regarding the single droplet evaporation process, which would provide a better fundamental understanding of droplet evaporation on surfaces undergoing high to intermediate superheating and heterogeneous wetting surface interfaces, is scarce.

2. Experiments

2.1. Experiment setup

A schematic of the experimental setup is presented in Fig. 1. A syringe was used to inject droplets at the required volume onto the heating surface of a copper column, and the droplet evaporation process was recorded using a charge-coupled device (CCD) camera. The drawing in Fig. 1 presents a detailed depiction of the droplets on the test copper surfaces. The diameter of the heating surface was 2 mm, and the water droplet (9 μL in diameter) was larger than the heating surface. The temperature of droplet before deposition on the test surfaces, referred to as the room temperature, was maintained constant through environmental control. The droplet evaporation process occurred in a controlled area. The surface temperature was measured using a thermocouple device positioned near the copper surface at a distance of 1 mm from the top. Since the thermal conductivity of the copper block is very high and the distance is only 1 mm from the surface, the estimate of surface temperature of error will be less than 0.01 °C. The surface temperature before droplet deposition on the test surfaces, referred to as the initial surface temperature T_w, was maintained constant through variation of the power supply and reached equilibrium after approximately 1 h. Evaporation experiments were performed at various maintained initial surface temperatures (120 ± 0.5 °C, 130 ± 0.5 °C, and 140 ± 0.5 °C).

2.2. Test surfaces

The three test surfaces (plain, hydrophilic, and mixed wettability) were used to investigate the effects of surface wettability on droplet evaporation, as depicted in Fig. 2. The water contact angle was measured with an optical contact angle meter. All CAs are measured before the tests, using Sindatek Model 100SB to produce schematic drawings of the CA meter. A drop volume of 9 μl which Bond number is 0.15 and capillary length is 2.74 mm was chosen for the measurements, and each region was examined using more than five values. The first test sample was a plain copper surface; it had a homogeneous wettability surface and a CA of approximately 95°. The scanning electron microscopy (SEM) image reveals the clean and smooth surface of plain copper. The second test sample (philic) was a homogeneous hydrophilic surface. The hydrophilic region was prepared using a nanosilica-particle–coated copper surface with a CA of approximately 41°. The nanoparticles were distributed uniformly on the substrate, as indicated in the SEM image. The sol–gel method with nanosilica particles was applied to modify the surface to achieve hydrophilic wettability [23,24]. The third test sample was a mixture of the first and second samples, and it was a surface with heterogeneous (mixed) wettability. The surface area is separated into two parts, namely the plain and hydrophilic regions, which are located on the right and left sides of the copper surface, respectively.

3. Results and discussion

3.1. Temperature curves of droplet evaporation on a superheated surface

Temperature is the primary factor that causes a sessile droplet to self-propel onto an intermediate superheating surface. The droplet motion resembles the Leidenfrost effect: water droplets can move on the surface after the temperature has increased to the Leidenfrost effect point (LFP) [25]. In this study, self-propelled sessile droplets on homogeneous plain and hydrophilic samples reached the LFP at surface temperatures of approximately 160 °C and 190 °C, respectively. On the surface with heterogeneous (mixed) wettability, similar motion of droplet occurred only at a temperature of approximately 140 °C, which is lower than the LFP we observed on the two homogenous surfaces. While we did not observe the Leidenfrost feature, a layer of vapor close to the surface, on the mixed patterned surface, we attribute the self-propelled droplet motion to another depinning mechanism provided by such pattern,

which is the main scope of the following discussion.

Temperature data indicated different trends for the surfaces with three types of wettability. The temperature curves of the three test surfaces with the initial surface temperatures of 120 °C (hollow symbols) and 140 °C (solid symbols) are presented in Fig. 3. In the cases with the initial surface temperatures of 120 °C, the surface temperature decreased because of contact with a cold droplet, and heat was transferred to the droplet until the temperatures of the surface and liquid had achieved equilibrium in the first phase. In the second phase, the temperature remained nearly constant (quasisteady temperature T′). In the end of droplet evaporation, the temperature rises to the initial surface temperatures. Compared to the results of quasisteady temperature for all three surfaces in Fig.3. There are mixed, philic and plain surfaces showing from high to low of quasisteady temperature. The surface with mixed wettability exhibited both the highest quasisteady temperature and the shortest evaporation time at initial surface temperatures of 120 °C and 140 °C. This implies that the dynamic behaviour of the liquid influenced the evaporation phenomena. This behaviour will discuss on the Part 3.4 of energy balance equation for droplet evaporation.

3.2. CCD Images of droplet evaporation on a superheated surface

The CCD images captured at 500 frames/s, displayed in Fig. 4, illustrate a self-propelled sessile droplet on a surface with heterogeneous wettability with an initial surface temperature set at 140 °C. At 0.6 s, the droplet began moving toward the hydrophilic region and gradually detached from the plain region. At the rightmost contact line, it began visibly moving to the left. The red arrow in the figure indicates the degree of displacement, which shows that the droplet reached the boundary of the interface at 0.9 s. The MCL caused the droplets to concentrate on the hydrophilic side; subsequently, some of the droplets were suspended at the periphery of the heating surface on the hydrophilic side. Due to the gravity force is increased in the process. Finally, the droplets rolled off the heating surface because of an imbalance in forces between gravity and surface tension. The duration for which a droplet remains on the heating surface is referred to as maxima time (t_{max}).

CA measurements may explain the relationship between different surface wetting characteristics that affect the movement of the contact line on a surface with mixed wettability. The droplets covered a larger area than the heating surface on top of the cylinder; therefore, the droplets remained confined to this limited heating surface area. The CA measurements when the droplets had stopped moving were approximately 120° on both sides. Because of the pinning effect at the edge, most of the evaporation is of the CCR (CCL) type, particularly for test samples with homogeneous wettability. Fig. 5 presents the variations of the CA on surfaces with mixed wettability at initial surface temperatures of 110–140 °C. When the surface temperature was maintained at a low superheat temperature (120 °C), the left and right sides exhibited a relatively equal CA. However, as the temperature increased beyond 140 °C, the surface initially maintained a difference in CA of 20° between the right and left sides because of the MCL and the right side of the contact line moved away from the edge. Before the droplet moved, the MCL caused the difference in CA to increase. More of the liquids were moved to the suspension of droplet by the gravity effect. The advancing contact angle in this situation is increased more than 180° and the RCA is decreased. In the final frame we can see a decrease of RCA, which is caused by the rolling off of the droplet. The length of time of the droplet motion is within 0.1 s, the droplet velocity is approximately 20 mm/sec. moving Compared with a low superheat temperature (120 °C), a higher superheat temperature (140 °C) resulted in a more noticeable difference in CA.

3.3. Force model for self-propelled sessile droplets

The droplet free body diagram displayed in Fig. 6 indicates the force composition that is primarily divided into gravity force (W) and surface tension force (F_σ). The horizontal surface tension force ($F_{\sigma H}$) of a sessile droplet self-propelled on a surface is similar to the lateral adhesion force [26,27] of a droplet sliding on an inclined surface. The left (hydrophilic) end can be considered the advancing angle, and the right (plain) end can be considered the receding angle. In this study, we observed that the horizontal surface tension force can move the contact line. The horizontal and vertical surface tension forces ($F_{\sigma H}$ *and* $F_{\sigma V}$) are determined by the difference between the right and left CAs on the surface, as indicated in Eq.s (1) and (2):

$$F_{\sigma H} = L\sigma(\cos\theta_r - \cos\theta_a) \quad (1)$$

$$F_{\sigma V} = L\sigma(\sin\theta_r + \sin\theta_a)/2 \quad (2)$$

where σ is the surface tension, L the contact line, θ_r the receding angle and θ_a the advancing angle. In Eq.s (2), because of the vertical surface tension acting on the contact line is uniform, we divide by two to express the concept of average.

Fig. 7a indicates that a high superheat temperature (140 °C) has a higher horizontal surface tension force ($F_{\sigma H}$) than that of a low superheat temperature (110–130 °C). Compared with a low superheat temperature, a high superheat temperature causes a greater difference in CA, which leads to a large horizontal surface tension force. However, the movement of droplets is also related to the vertical surface tension force ($F_{\sigma V}$). Fig. 7b indicates that a high superheat temperature can reduce the vertical surface tension force. This implies that the pinning effect of a droplet decreases as the superheat temperature increases. For example, for the case of 140 °C, we observed that the most substantial decrease in the pinning effect occurred at the location where the contact line had moved. We determined that the pinning effect resulting from changes in

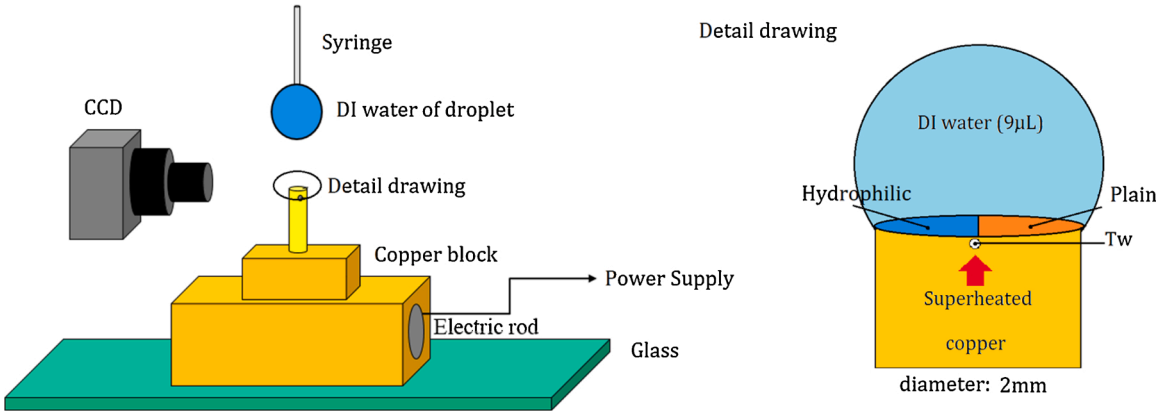

Fig. 1. (a) Experimental setup of droplets on a superheated and spatially restricted surface and details regarding the heating surfaces at different wettability levels.

the vertical surface tension force can cause the contact line to move.

In Yadav's research [28], they found the initial increase rate of retention force is high due to surface deformation induced by unsatisfied normal force, which might indeed play a role on our asymmetric surface wetting pattern. However, considering we have different setting than Yadav, namely the rigorous evaporation and the fact our droplet pinned by the edge of the surface, we can't be certain how much the time effect contributes to the motion. For the case the evaporation started immediately after the deposition, and the evaporation completed within few secs. The effect of rested time on the retention force of droplet in this study is small. Continuous heating causes the right contact line to move to the interface in the middle of the surface, and most liquid is squeezed into the hydrophilic region. At this time, the hydrophilic region cannot accommodate all the liquid, and some of it moves toward the heating surface. The weight of the volume of liquid contained outside the heating surface region (V_{out}) is W_{out}, and the weight of the volume of the liquid at the heating surface (V_{in}) is W_{in}, as shown in Eq.s (3) and (4), respectively. Consideration of the influence of bubbles inside the droplet, volume of bubble is deducted from the calculation of W_{in}. Fig. 8 displays the relationships of torque with W and F_{σ}. If the leftmost point on the heating surface is taken as the fulcrum, then when the counterclockwise torque caused by W_{out} is greater than the clockwise torque of the vertical surface tension force ($F_{\sigma V}$) and W_{in}, the droplet instantly rolls off the heating surface.

$$W_{in} = \rho g V_{in} \tag{3}$$

$$W_{out} = \rho g V_{out} \tag{4}$$

3.4. Energy balance equation for droplet evaporation

The behaviour of a self-propelled sessile droplet on a superheated and heterogeneous wetting surface can be explained by energy balance theory. When droplet evaporation is complete, the required energy can be classified as the energy expended during phase change; therefore, the energy expended during droplet evaporation can be calculated using the latent heat. The energy is indicated in Eq. (5), where m is the mass of the droplet and h_{fg} the enthalpy of the droplet during evaporation. In addition, droplet evaporation caused the surface temperature on the copper column to decrease. We can calculate the energy expended as the droplet cools the copper column by using Eq. (6), where m_{copper} is the mass of copper, C the specific heat, T the steady initial surface temperature, and T′ the quasisteady temperature in the second phase.

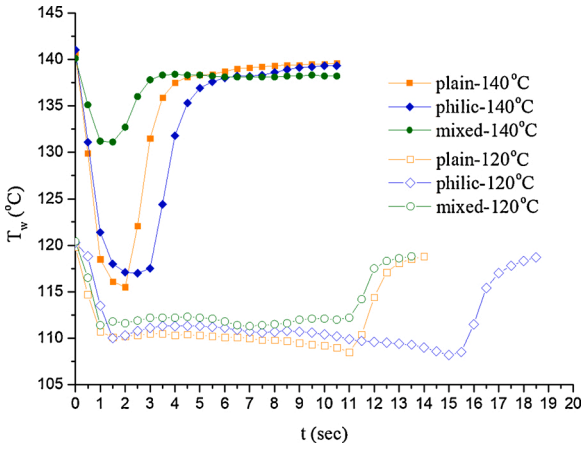

Fig. 3. Temperature plotted against time for surfaces with three wettability types (plain, hydrophilic, and mixed wettability) at initial surface temperatures of 120 °C (hollow symbols) and 140 °C (solid symbols).

$$E_{droplet} = mh_{fg} \tag{5}$$

$$E_{copper} = m_{cooper} C\left(T - T^{'}\right) \tag{6}$$

The relationship between the energy expended during droplet evaporation and that expended as the droplet cools for the three test surfaces is presented in Fig. 9. According to energy balance theory, the energy expended during droplet evaporation (Eq.5) should be equal to the energy expended as the droplet cools a surface (experiment data, Eq.6). Some of these energy conversions may be caused by irreversibility; however, in this study, we suggest that most of the energy conversion may be caused by liquid-to-gas phase changes. The three energy curves (Eq. 6) for the droplet cooling the surface do not overlap with those of droplet evaporation (Eq. 5). We observed a difference in the energy expended as the superheat temperature increased between that calculated using Eq. (5) and that calculated using experimental data in

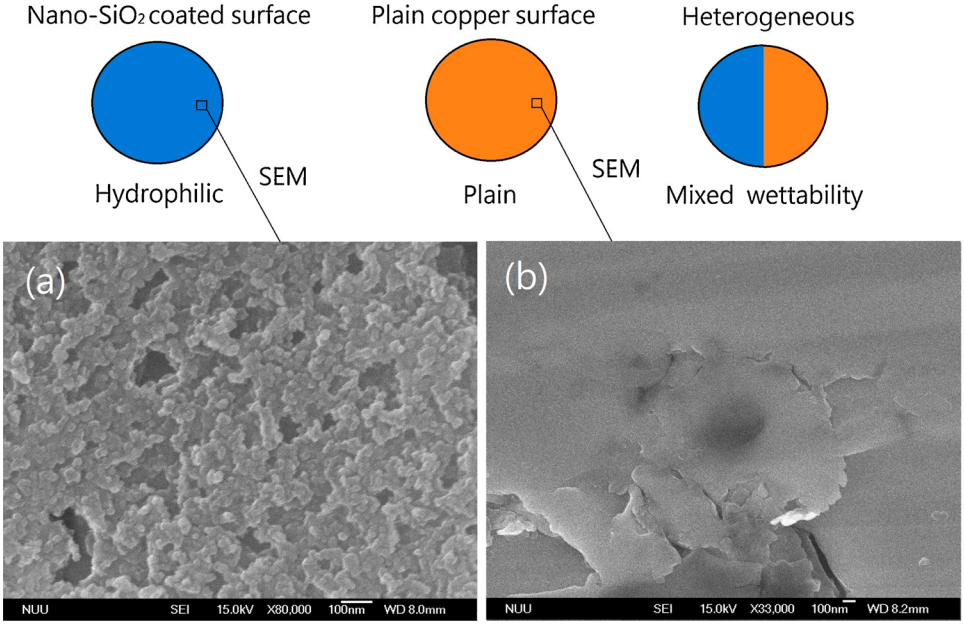

Fig. 2. Scanning electron microscopy images of the (a) nano-SiO_2–coated surface at a magnification of 80,000× and (b) plain surface at a magnification of 190,000 × .

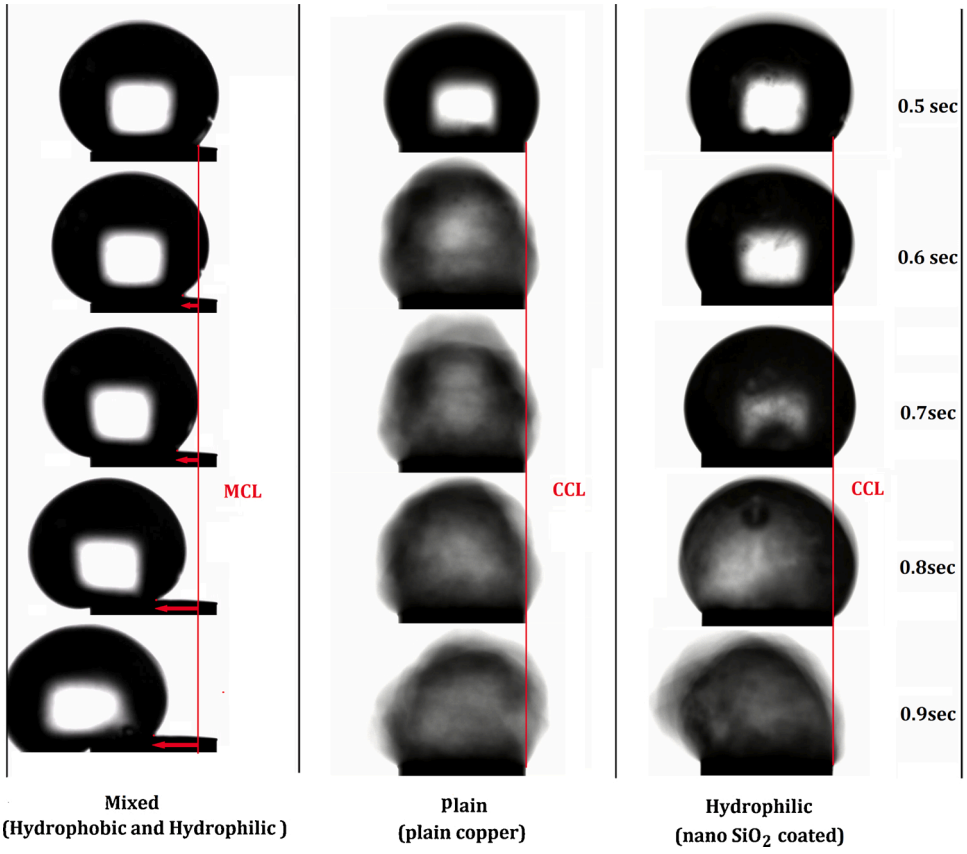

Fig. 4. Charge-coupled device images illustrating different evaporation behaviours on the surfaces with heterogeneous wettability (mixed) and homogeneous wettability (plain and hydrophilic) at an initial surface temperature of 140 °C. On the surface with mixed wettability, the droplet had a moving contact line after exhibiting static unbalance. However, the homogeneous surfaces had a constant contact line with a greater amount of evaporation.

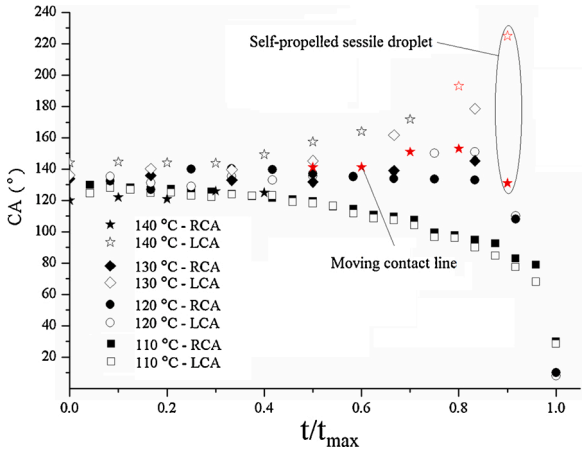

Fig. 5. Maxima time plotted against contact angles (CAs) of droplets evaporating on a surface with mixed wettability at initial surface temperatures of 110–140 °C. Solid symbols are on the right side of the CA, and hollow symbols are on the left side of the CA. Red color symbol shows the moving contact line MCL. In the case of mixed surface at 140 °C, before the droplets rolled off, some of the liquids were suspended at the periphery of the hydrophilic side. The advancing contact angle in this situation is increased more than 180° and receding contact angle is decreased.

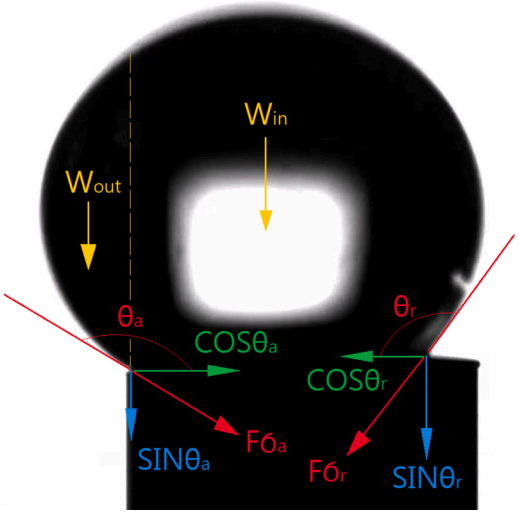

Fig. 6. Force model of a self-propelled sessile droplet.

Eq. (6). This is attributable to an increase in the intensity of bubble generation as the superheat temperature increased. In addition, surface wetting characteristics contributed to greater changes in energy on surfaces with heterogeneous wettability than on other uniform surfaces. Our previous study [22] reported the images of droplet evaporation on the three kinds of surfaces. Hydrophilic surface had least enclosed vapor generation in the evaporation process, and the difference of energy between surface cooling (by Eq. 6) and droplet evaporation (by Eq.5) is smaller. Compared to the other two surfaces, the bubble motion is intensively, the greater difference in the energy between Eq.5 and Eq. 6, especially in the surface with mixed wettability. It aligns well with our finding in Fig. 9 that energy difference between droplet evaporation and surface cooling is largest for mixed case and smallest for hydrophilic one, we speculate such energy difference reflects the kinetic energy of

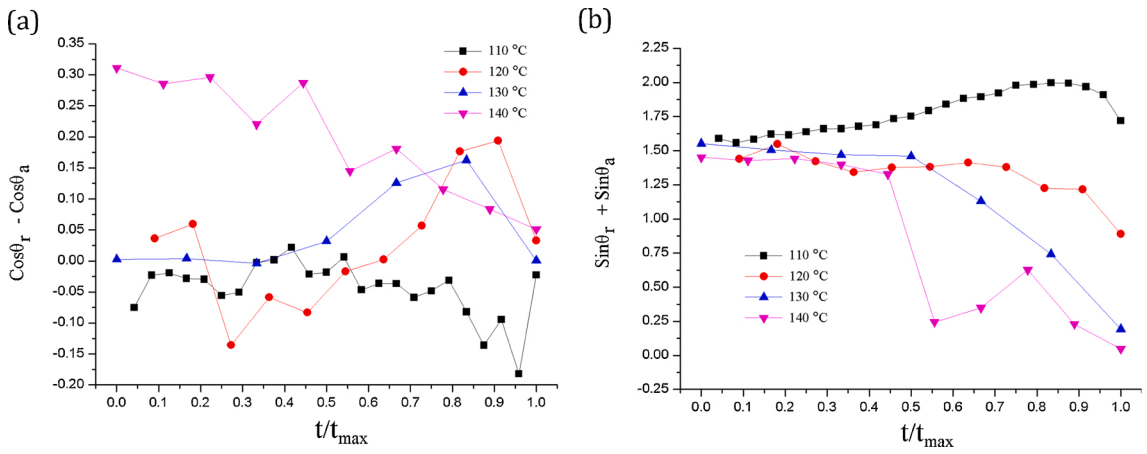

Fig. 7. Maxima time at contact angles of groups(a) $\cos\theta_r - \cos\theta_a$ and (b) $\sin\theta_r + \sin\theta_a$ for droplets evaporating on a surface with mixed wettability at initial surface temperatures of 110–140 °C.

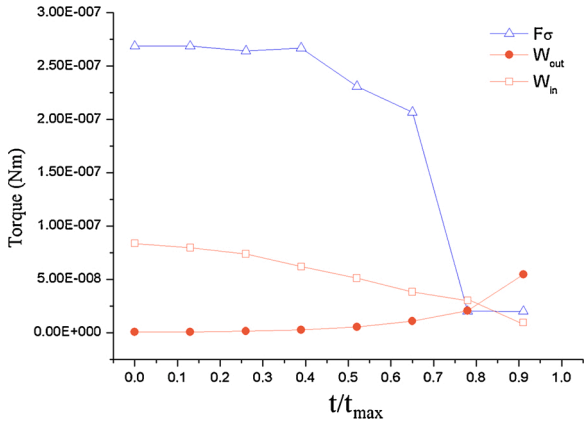

Fig. 8. Maxima time plotted against torque in relation to W and F_σ for a droplet evaporating on a surface with mixed wettability at an initial surface temperature of 140 °C.

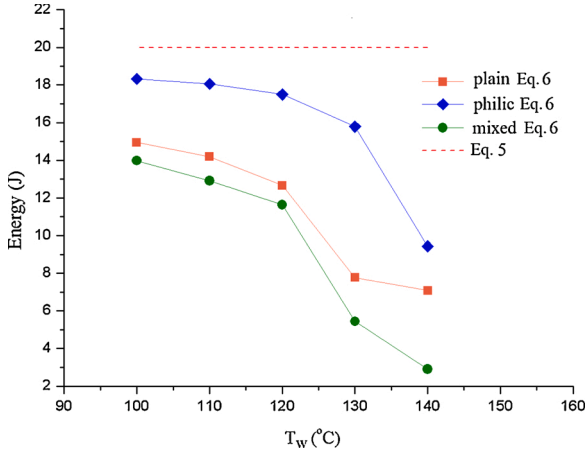

Fig. 9. Relationship of superheat temperature to the energy coming into and out of the system for surfaces with three types of wettability (plain, hydrophilic, and mixed wettability). Energy coming into the system was calculated using Eq. (5), and energy leaving the system was calculated using Eq. (6). Each symbol has four parameters that correspond to initial surface temperatures.

droplet motion on the mixed surface. These two findings indicate that high temperatures and mixed wettability cause large differences in energy and thereby significantly affect the dynamic liquid–vapour behaviour inside a droplet.

4. Conclusion

At an extremely high superheat temperature, the dynamic liquid–vapour behaviour inside a droplet changes. Because of a considerable difference in energy, the sessile droplet self-propelled on the heterogeneous wetting surface in advance. Therefore, we infer that an increase in temperature is the primary factor affecting liquid–vapour dynamic behaviour. However, if wetting characteristics are combined to form a surface with mixed wettability, the liquid–vapour dynamic behaviour is significantly increased. This confirms that surface temperatures within the moderate-to-high superheat temperature range are correlated with liquid–vapour phase transition, which is crucial for liquid–vapor heat transfer, particularly on surfaces with mixed wettability.

CRediT authorship contribution statement

Chin-Chi Hsu: Data curation, Writing - original draft. **You-An Lee:** Writing - review & editing. **Chun-Hui Wu:** Visualization, Investigation. **C.S. Sujith Kumar:** Supervision.

Declaration of Competing Interest

The authors declare that they have no known competing financial interests or personal relationships that could have appeared to influence the work reported in this paper.

Acknowledgements

The authors gratefully acknowledge funding provided by the Ministry of Science and Technology (grant numbers: MOST 106-2221-E-239 -016 and MOST 105-2221-E-239 -015). This manuscript was edited by Wallace Academic Editing.

References

[1] P. Calvert, Inkjet printing for materials and devices, Chem. Mater. 13 (2001) 3299–3305.
[2] J. Lim, W. Lee, D. Kwak, K. Cho, Evaporation-induced self-organization of inkjet-printed organic semiconductors on surface-modified dielectrics for high-performance organic transistors, Langmuir 25 (9) (2009) 5404–5410.
[3] J. Park, J. Moon, Control of colloidal particle deposit patterns within picoliter droplets ejected by ink-jet printing, Langmuir 22 (8) (2006) 3506–3513.

[4] A. Ebrahimi, P. Dak, E. Salm, S. Dash, S.V. Garimella, R. Bashir, M.A. Alam, Nanotextured superhydrophobic electrodes enable detection of attomolar-scale DNA concentration within a droplet by non-faradaic impedance spectroscopy, Lab Chip 13 (21) (2013) 4248–4256.
[5] C. Rivet, H. Lee, A. Hirsch, S. Hamilton, H. Lu, Microfluidics for medical diagnostics and biosensors, Chem. Eng. Sci. 66 (7) (2011) 1490–1507.
[6] V. Dugas, J. Broutin, E. Souteyrand, Droplet evaporation study applied to DNA chip manufacturing, Langmuir 21 (20) (2005) 9130–9136.
[7] S.T. Chang, O.D. Velev, Evaporation-induced particle microseparations inside droplets floating on a chip, Langmuir 22 (4) (2006) 1459–1468.
[8] A.G. Pautsch, T.A. Shedd, Spray impingement cooling with single-and multiple-nozzle arrays. Part I: Heat transfer data using FC-72, Int. J. Heat Mass Transf. 48 (15) (2005) 3167–3175.
[9] N. Kumari, S.V. Garimella, Characterization of the heat transfer accompanying electrowetting or gravity-induced droplet motion, Int. J. Heat Mass Transf. 54 (17–18) (2011) 4037–4050.
[10] H.K. Dhavaleswarapu, C.P. Migliaccio, S.V. Garimella, J.Y. Murthy, Experimental investigation of evaporation from low-contact-angle sessile droplets, Langmuir 26 (2) (2010) 880–888.
[11] R.G. Picknett, R. Bexon, The evaporation of sessile or pendant drops in still air, J. Colloid Interface Sci. 61 (2) (1977) 336–350.
[12] D.H. Shin, S.H. Lee, J.Y. Jung, J.Y. Yoo, Evaporating characteristics of sessile droplet on hydrophobic and hydrophilic surfaces, Microelectron. Eng. 86 (4–6) (2009) 1350–1353.
[13] K.S. Birdi, D.T. Vu, Wettability and the evaporation rates of fluids from solid surfaces, J. Adhes. Sci. Technol. 7 (6) (1993) 485–493.
[14] S. Dash, S.V. Garimella, Droplet evaporation on heated hydrophobic and superhydrophobic surfaces, Phys. Rev. E 89 (2014), 042402.
[15] N.T. Pham, G. McHale, M.I. Newton, B.J. Carroll, S.M. Rowan, Application of the quartz crystal microbalance to the evaporation of colloidal suspension droplets, Langmuir 20 (3) (2004) 841–847.
[16] E. Bonaccurso, H.J. Butt, Microdrops on atomic force microscope cantilevers: evaporation of water and spring constant calibration, J. Phys. Chem. B 109 (1) (2005) 253–263.
[17] M. Lee, D. Lee, N. Jung, M. Yun, C. Yim, S. Jeon, Evaporation of water droplets from hydrophobic and hydrophilic nanoporous microcantilevers, Appl. Phys. Lett. 98 (1) (2011), 013107.
[18] D.L. He, Q. Huihe, Multicomponent droplet evaporation on chemical micro-patterned surfaces, Sci. Rep. 7 (2017) 41897.
[19] Qing-Li P. Zhou, H.J. Yan, Pinning–depinning mechanism of the contact line during evaporation on chemically patterned surfaces: a lattice Boltzmann study, Langmuir 32 (37) (2016) 9389–9396.
[20] H.P. Jansen, J.W.H. Zandvliet, E.S. Kooij, Evaporation of elongated droplets on chemically stripe-patterned surfaces, Int. J. Heat Mass Transf. 82 (2015) 537–544.
[21] M. He, D. Liao, H. Qiu, Multicomponent droplet evaporation on chemical micro-patterned surfaces, Sci. Rep. 7 (2017) 41897.
[22] C.C. Hsu, T.W. Su, C.H. Wu, L.S. Kuo, P.H. Chen, Influence of surface temperature and wettability on droplet evaporation, Appl. Phys. Lett. 106 (2015), 141602.
[23] M.Y. Tsai, C.C. Hsu, P.H. Chen, C.S. Lin, A. Chen, Surface modification on a glass surface with a combination technique of sol–gel and air brushing processes, Appl. Surf. Sci. 257 (20) (2011) 8640–8646.
[24] C.C. Hsu, T.W. Su, P.H. Chen, Pool boiling of nanoparticle-modified surface with interlaced wettability, Nanoscale Res. Lett. 7 (2012) 259.
[25] M. Shirota, M.A.J. van Limbeek, C. Sun, A. Prosperetti, D. Lohse, Dynamic Leidenfrost effect: relevant time and length scales, Phys. Rev. Lett. 116 (2016), 064501.
[26] D.W. Pilat, P. Papadopoulos, D. Schäffel, D. Vollmer, R. Berger, H.J. Butt, Dynamic measurement of the force required to move a liquid drop on a solid surface, Langmuir 28 (49) (2012) 16812–16820.
[27] S.Y. Bekir, A.S. Abudllah, A. Haider, A.A. Nasser, Fabrication of Co_3O_4 nanoparticles in thin porous carbon shells from metal–organic frameworks for enhanced electrochemical performance, RSC Adv. 7 (2017) 13340–13346.
[28] P.S. Yadav, P. Bahadur, R. Tadmor, K. Chaurasia, A. Leh, Drop retention force as a function of drop size, Langmuir 24 (2008) 3181–3184.